Front. Chem. Sci. Eng. 2021, 15(4): 922–934
https://doi.org/10.1007/s11705-020-2004-z

RESEARCH ARTICLE

Molecular dynamics simulation on DNA translocating through MoS_2 nanopores with various structures

Daohui Zhao[1,2], Huang Chen[1], Yuqing Wang[2], Bei Li[2], Chongxiong Duan[3], Zhixian Li[1], Libo Li (✉)[1]

1 School of Chemistry and Chemical Engineering, South China University of Technology, Guangzhou 510640, China
2 School of Chemistry and Chemical Engineering, Hubei University, Wuhan 430062, China
3 School of Materials Science and Hydrogen Energy, Foshan University, Foshan 528231, China

© Higher Education Press 2021

Abstract The emergence of MoS_2 nanopores has provided a new avenue for high performance DNA sequencing, which is critical for modern chemical/biological research and applications. Herein, molecular dynamics simulations were performed to design a conceptual device to sequence DNA with MoS_2 nanopores of different structures (e.g., pore rim contained Mo atoms only, S atoms only, or both Mo and S atoms), where various unfolded single-stranded DNAs (ssDNAs) translocated through the nanopores driven by transmembrane bias; the sequence content was identified by the associating ionic current. All ssDNAs adsorbed onto the MoS_2 surface and translocated through the nanopores by transmembrane electric field in a stepwise manner, where the pause between two permeation events was long enough for the DNA fragments in the nanopore to produce well-defined ionic blockage current to deduce the DNA's base sequence. The transmembrane bias and DNA-MoS_2 interaction could regulate the speed of the translocation process. Furthermore, the structure (atom constitution of the nanopore rim) of the nanopore considerably regulated both the translocate process and the ionic current. Thus, MoS_2 nanopores could be employed to sequence DNA with the flexibility to regulate the translocation process and ionic current to yield the optimal sequencing performance.

Keywords DNA sequencing, MoS_2, molecular dynamics simulation, nanopore, ionic current

1 Introduction

Nanopore-based DNA sequencing [1–5] provides a new approach for rapid, high-resolution detection of DNA bases (guanine (G), adenine (A), thymine (T) and cytosine (C)). The negatively charged DNA molecules could be driven electrophoretically through a nanopore by an applied external voltage [6]. Protein nanopores [7,8] and solid-state nanopores [9–12] have been widely studied for DNA sequencing. However, these pores are limited by low signal-to-noise ratio (SNR) and nonuniform single-base sequencing and are too thick to identify individual bases in the DNA sequence. Furthermore, biological nanopores are prone to disassemble at high biases [13,14]. Such drawbacks can be overcome by developing new two-dimensional materials for nanopore sequencing, such as graphene [15–18] and MoS_2 [19–21], which have attracted extensive attention due to their ultrathin atomic thickness that allows sequencing with single-base resolution. The merits of this type of device are mainly twofold: 1) the film can amplify the baseline and signal amplitude without increasing the noise level, which can greatly improve the SNR; 2) ultra-small and short nanopores can enhance detection accuracy. Graphene, a two-dimensional (2D) nanomaterial, has been studied extensively for DNA sequencing [22]. The single-atom-thick graphene nanopores allow single-base detection by blocking ionic currents or lateral tunneling currents. However, graphene nanopores have some shortcomings: the lack of band gap for applications such as charged base detection and field effect transistors; strong π-π interaction with DNA [23]; and low detection of SNR. Thus, there is an emergent need to find graphene substitutes or modify graphene to achieve a good sensing performance and a non-adhesive surface, for the development of next-generation DNA sequencing equipment. MoS_2, a 2D single-layer structure analogous to graphene, has found a wide range of applications in sensing, nanoelectronics, and energy storage, among others [24]. The thickness of single-layer MoS_2 is ~6.5 Å, which is comparable to the spacing between two

Received June 20, 2020; accepted August 6, 2020

E-mail: celbli@scut.edu.cn

adjacent bases of ssDNA (3.2–3.5 Å). Previous studies have revealed that MoS_2 has several advantages over graphene with improved SNR [19,20] and controllable fabrication of nanopores [24,25], suggesting MoS_2 as a promising material for DNA sequencing. Single-layer MoS_2 can be regarded as an "S-Mo-S" sandwich structure, with each Mo coordinating with six S atoms in a trigonal prismatic geometry. Meanwhile, the Mo atom of MoS_2 is hydrophilic, and the S atom is hydrophobic. There are three types of MoS_2 nanopores: Mo atoms only (Mo only), S atoms only (S only), and both Mo and S atoms at the edge of the nanopore (Mixed) [26]. Thus, the type of atom (Mo, S or both) of the MoS_2 nanopore edge exposed to DNA bases may lead to interactions with DNA that are different from that of graphene. Both experimental and simulation studies have proven that DNA does not adsorb strongly to the MoS_2 surface [19,20]. It also has been reported that aromatic compounds (e.g., pyridine and purine) or conjugated compounds could physically adsorb to MoS_2 surface [27].

Molecular dynamics (MD) simulations can provide details at the atomic level for the translocation dynamics of different molecules, such as ions and biomolecules, and their interactions with nanopores [28–38]. For example, DNA sequencing using graphene nanopores was investigated by Liang et al. [39], and the relationship between ion current blockade and the nanopore area occupied by DNA translocation was revealed. Heiranian et al. [26] used MD simulations to study the desalination effect of MoS_2 nanopores and found that different nanopores showed different effects in modulating the water flux. The water flux of Mo only nanopores was 70% higher than that of graphene nanopores with the same pore diameter. In addition, Farimani et al. [20] performed a density functional theory calculation to compare the performance of these three MoS_2 pores in detecting the four different bases. They showed that Mo atoms interacted with DNA bases more weakly than S atoms, leading to promising potential for Mo only nanopores to discriminate DNA bases. Luan and Zhou [32] investigated the spontaneous transport of ssDNA through a heterostructure of graphene-MoS_2 nanopore under the chemical potential difference.

Since MoS_2 consists of metal and non-metal atoms, the Mo:S ratio could be adjusted around the MoS_2 nanopore edge [38]. Thus, the MoS_2 nanopore's structure is expected to regulate the ssDNA's motion and ionic current, which provides new possibilities to enhance the performance of DNA sequencing. Consequently, we examined the translocation characteristics of stretched ssDNA through three different types of MoS_2 nanopores. We analyzed the characteristics of three open nanopores and studied the interaction of ssDNA with the MoS_2 surface and its translocating through the three nanopores. Following the introduction, the atomistic models of three MoS_2 nanopores and ssDNA structure, as well as the simulation methods are elaborated in section 2, "Experimental". In section 3, "Results and discussion", the ionic currents and electrostatic potentials for the three MoS_2 nanopores are presented, and the interaction of ssDNA with them are examined. Then, the process of ssDNA passing through different MoS_2 nanopores is analyzed. Section 4 presents the concluding remarks.

2 Experimental

2.1 System setup

Four homogeneous ssDNAs, each with 20 bases (i.e., $poly(A)_{20}$, $poly(T)_{20}$, $poly(G)_{20}$, and $poly(C)_{20}$), were studied. To simulate the four stretched ssDNAs passing through MoS_2 nanopores under an applied electric field, several simulation systems have been constructed, each containing a single-layer MoS_2 membrane with a pore diameter of 1.6 nm, a 20-base ssDNA and 1 $mol \cdot L^{-1}$ KCl solution. The pore diameter of 1.6 nm was chosen so that ssDNA could pass through the pore at a moderate speed while significantly blocking the ionic current [30,39]. Fig. 1 illustrates the schematic diagrams of initial configuration and a ssDNA translocating through MoS_2 nanopores. For the atoms exposed at the nanopore rim, the three nanopores were denoted as Mo only, S only and Mixed nanopore: e.g., the rim of the Mo only nanopore exposed only Mo atoms (thus bore positive charge), while that of the Mixed nanopore exposed both Mo and S atoms (Mo:S = 1:2). Since more S or Mo atoms are etched from the edge of the Mixed nanopore to produce Mo, or S only nanopores, the area of the nanopore is slightly larger than the Mixed nanopore. The nanopore diameter, calculated as $d = 2 \times \sqrt{S/\pi}$ (S is the nanopore area), for Mo, S, and Mixed nanopore are 1.91, 1.75, 1.62 nm, respectively. The ssDNAs were constructed by the avogadro software [40], and the MoS_2 nanopores were built as described in the literature [41]. The DNA-MoS_2 system was placed in a box of 7.59 nm × 7.66 nm × 10.00 nm and then solvated with TIP3P (transferable intermolecular potential with 3 points) water molecules [42]. Potassium (K^+) and chloride (Cl^-) ions were added to make the system electrically neutral, yielding a 1 $mol \cdot L^{-1}$ KCl electrolyte. The entire simulation system contained approximately 50000 atoms.

2.2 MD simulations

All MD simulations were carried out by the GROMACS 4.6.7 software [43] with CHARMM27 force field [44], and the analysis and visualization were conducted with GROMACS utilities and VMD software [45]. The force field parameters for MoS_2 have been published in previous work [46] and validated by various MD simulations on nanopore sensing [30–32]. The LINCS [47] algorithm was

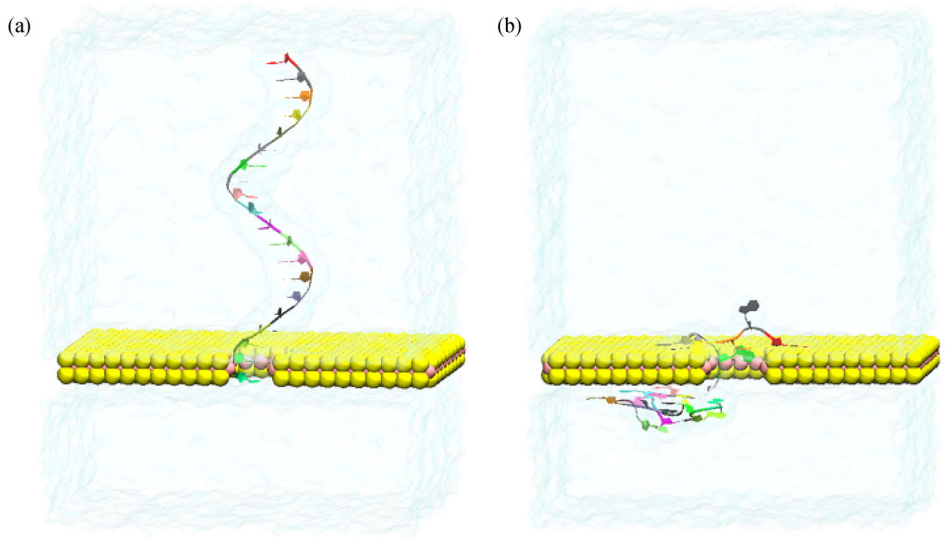

Fig. 1 The schematic diagrams of (a) initial configuration of the simulation system and (b) a poly(A)$_{20}$ translocating through the MoS_2 nanopore. The Mo atoms are colored in cyan, and the sulfur atoms are in yellow. The bases of poly(A)$_{20}$ are assigned different colors, and the ions are omitted for the sake of clarity.

applied to constrain the bonds that contain hydrogen atoms, and the SETTLE algorithm [48] was applied for water molecules. Due to the rigidity of MoS_2, the surface was frozen during the simulations [32,49]. For the non-bonded interactions between different types of atoms, the Lennard-Jones (LJ) parameters were obtained using the Lorentz-Berthelot [50] mixing rule. The LJ interactions were truncated by a switching function in the range of 1.1–1.2 nm, with a dispersion correction applied. The particle-mesh Ewald method [51] was used to compute the long-range electrostatic interactions. Periodic boundary conditions were used in all three dimensions.

The system was initially energy-minimized for 10000 steps using the steep descent method and then equilibrated in an isobaric-isothermal ensemble for 10 ns, in which the skeletal atoms of ssDNA were harmonically constrained with a force constant of 1000 kJ·mol^{-1}·nm^{-2}. The system temperature was maintained at 300 K by a V-rescale [52] thermostat and pressure at 1.0 bar with a semi-isotropic Berendsen [53] barostat along the z direction. After that, the system was equilibrated in canonical (NVT) ensemble for 120 ns at 300 K with the Nose-Hoover [54] thermostat, where the harmonical constraint was applied to only one backbone atom of the ssDNA in the nanopore (other ssDNA atoms could move freely). Production simulations were run in the NVT ensemble with electric field applied along the z direction, where ssDNA was not restrained. The external electric field was represented by the transmembrane voltage difference $V = -EL_z$, where E indicated the electric filed strength and L_z was the length of the simulation box along the z direction. The integration time step was 2 fs, and other simulation details are available in previous publications [30,55–57].

2.3 Data analysis

The number of bases adsorbed on the MoS_2 surface was analyzed by counting the bases whose center of mass distance followed a 6 Å threshold of the nearest S atom from the MoS_2 surface. The number of contacts was counted as the number of ssDNA atoms whose distance to MoS_2 membrane was less than 6 Å. The distance criterion of 6 Å was chosen to maintain consistency with our previous work [30], where distance criterion ranging from 5 to 9 Å yielded similar results. The number of translocated bases, N, was computed by counting the number of bases passing through the MoS_2 nanopore, and the slope of N versus t, the simulation time, was calculated as the translocation rate. The time series of ionic current $I(t)$ through MoS_2 nanopore were computed using the following equation:

$$I(t) = \frac{1}{\Delta t L_z} \sum_{i=1}^{N} q_i [z_i(t + \Delta t) - z_i(t)].$$

where Δt was 2 ps, q_i and z_i were the charge and z coordinate of the ith ion, respectively, and N was the total number of ions. To reduce noise, the time series of ionic current were block-averaged [58].

3 Results and discussion

3.1 Ionic current through three types of MoS_2 nanopores

To characterize the three types of open MoS_2 nanopores (Mo only, S only and Mixed), a series of voltages ranging from 0.5 to 2.4 V were simulated, where the system

contained a MoS_2 nanopore and 1 mol·L^{-1} KCl solution only. Each MD run lasted 20 ns, and the open-pore ionic currents for the MoS_2 nanopores are shown in Fig. 2(a). It was observed that under the same voltage, the S only nanopore produced the largest ionic current, followed by Mo only and Mixed nanopore. For instance, at the biased voltage of 1.2 V, the open ionic currents of S only nanopore, Mo only nanopore and Mixed nanopore were 5.41, 4.22 and 3.37 nA, respectively. In addition, the conductance was calculated from linearly fitting the I–V characteristic curve. It can be seen that the order of conductance is S only > Mixed > Mo only. Figure 2(b) shows the instantaneous electrostatic potential of the ion distribution around a MoS_2 nanopore with a bias of 1.2 V, where the point charge was approximated as a Gaussian sphere. Furthermore, the electrostatic potential over the pore in the x and y directions was averaged to yield the electrostatic potential profile across the pore along the z axis (Fig. 2(c)). The potential decreased from 0.1 to –1.1 V mainly across the nanopore and reached constants at both ends of the simulation box, as illustrated in Figs. 2(b) and 2(c). Note that similar behaviors were seen in previous studies [59,60].

3.2 Interaction of ssDNA with MoS_2 surface

Figure 3 compares the adsorption process for four different unfolded ssDNA on MoS_2 surface. During the simulation, the ssDNA molecules were initially placed at least 0.5 nm above the MoS_2 surface, and it was found that the four ssDNAs all adsorbed onto the MoS_2 surface, which was in accordance with Liang's results [41]. As illustrated in Fig. 3(a), several bases of polynucleotide lied parallel to the MoS_2 surfaces to maximize the van der Waals interaction, though there are no delocalized π electrons in MoS_2 to form the π-π stacking interaction similar to that in graphene. Furthermore, the number of DNA bases adsorbed on the surface, the number of base-to-surface

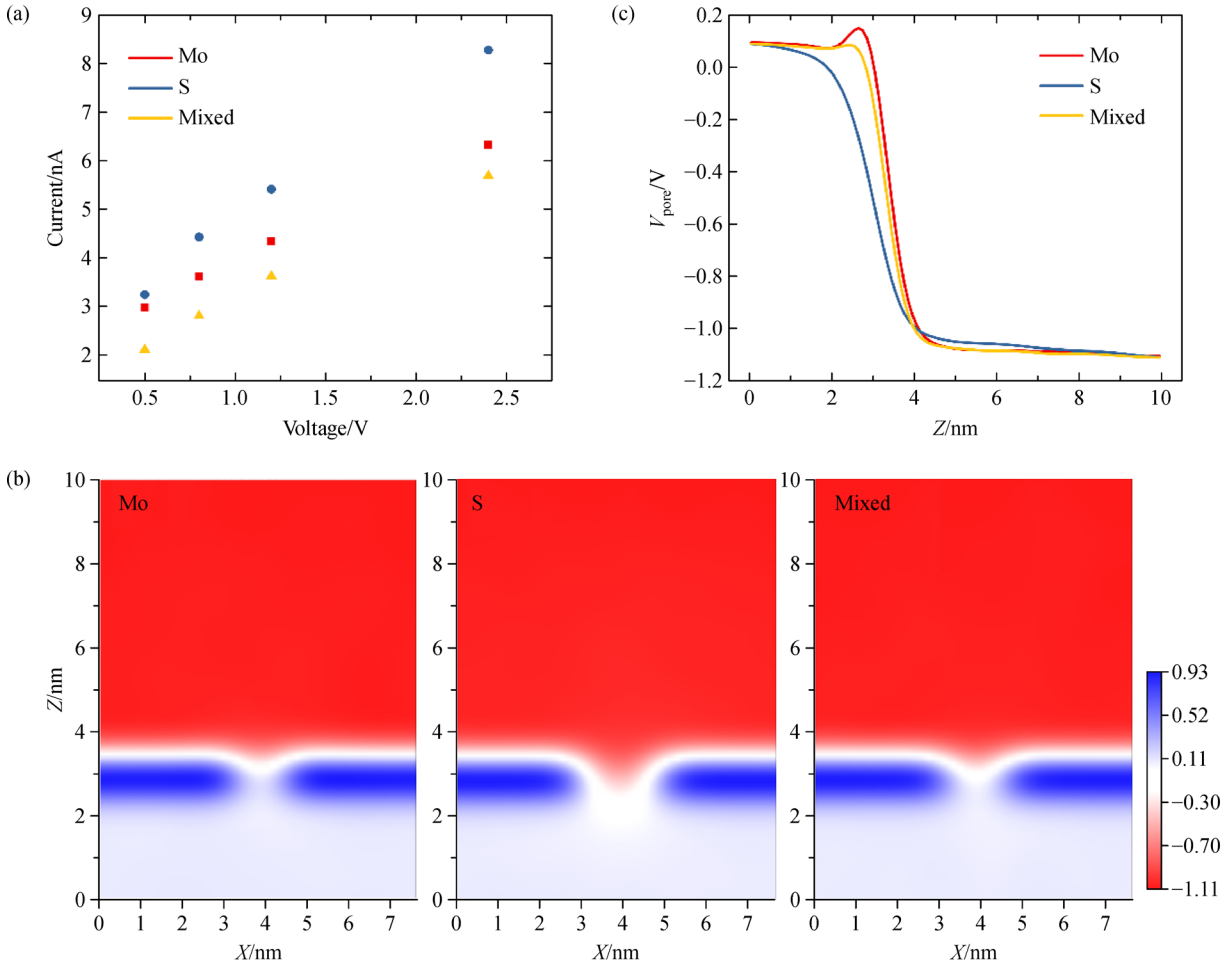

Fig. 2 (a) I–V profiles of three MoS_2 nanopores: Mo only, S only and Mixed; (b) electrostatic potential map for three MoS_2 nanopores under an external bias of 1.2 V (All point charges were approximated by Gaussian spheres with an inverse width $\beta = 0.25$ Å^{-1}. The charge of Mo or S only nanopore rim may change the electrical potential in the nanopore; thus, the nanopore size in the electrostatic potential map may be different from the actual physical size); (c) the average electrostatic potential profile across the pore along the z axis for three MoS_2 nanopores at 1.2 V bias.

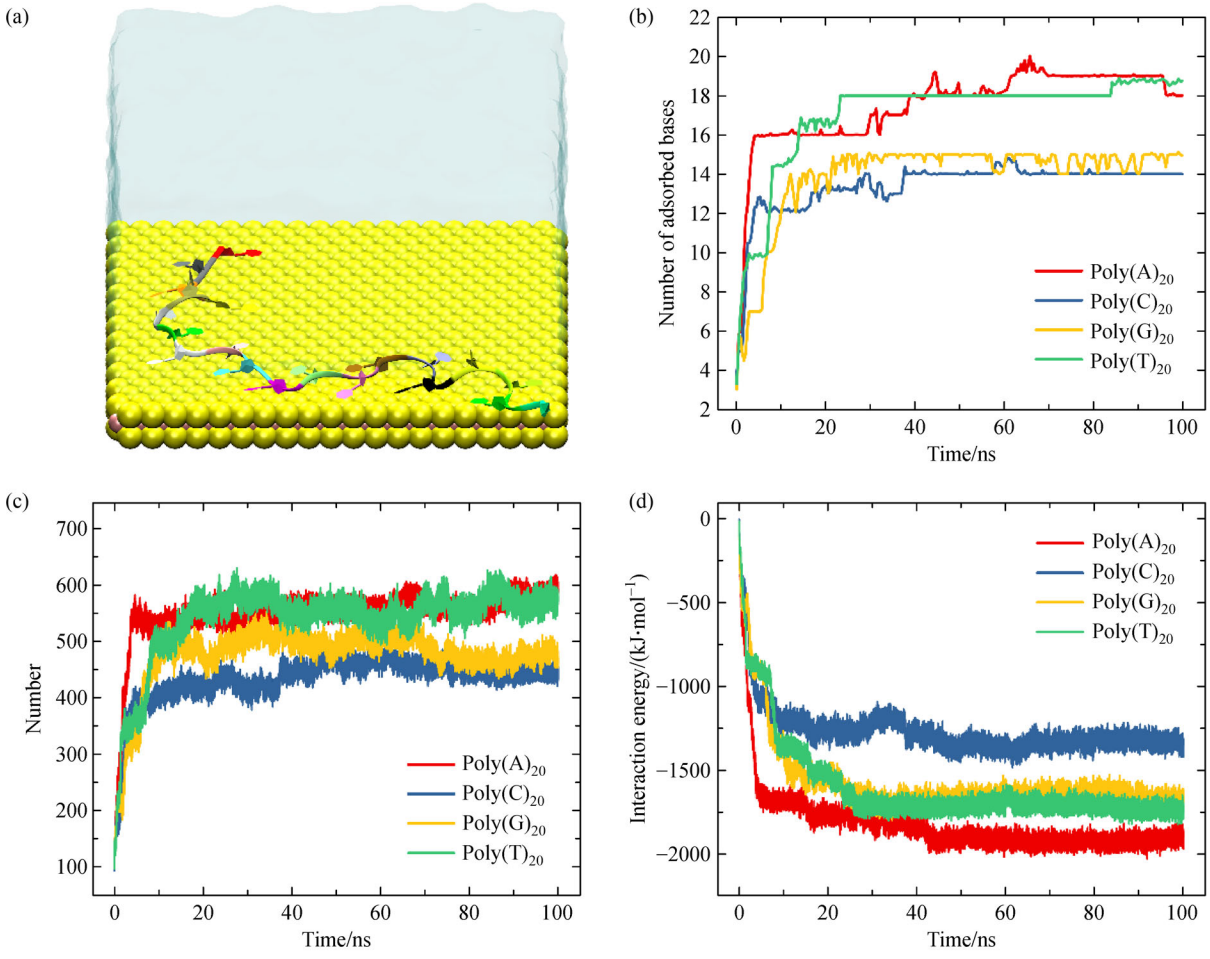

Fig. 3 ssDNA interacts with MoS_2 surface. (a) The snapshot of poly(C)$_{20}$ adsorbed onto MoS_2 surface (The MoS_2 is represented by van der Waals spheres: yellow (S) and cyan (Mo). The bases are represented by the NewRibbons model); (b) the adhesion number between ssDNA and the MoS_2 surface; (c) the number of contacts between ssDNA and the MoS_2 surface; (d) time series for the interaction energies between ssDNA and MoS_2 surface.

contacts, and the interaction energy between them were analyzed over the simulation time. As shown in Fig. 3(b), the number of adsorbed bases of the four ssDNAs all increased to above 12 within 10 ns. The equilibrium adsorption numbers of poly(A)$_{20}$ and poly(T)$_{20}$ were close to 18, and those of poly(C)$_{20}$ and poly(G)$_{20}$ were ~14. The order of adsorption base number was poly(A)$_{20}$ > poly(T)$_{20}$ > poly(G)$_{20}$ > poly(C)$_{20}$. The number of base-to-surface contacts between ssDNA and MoS_2 surface followed the similar order (Fig. 3(c)) as the number of adsorbed bases (Fig. 3(b)). The contact numbers for poly(A)$_{20}$ and poly(T)$_{20}$ were ~550, and those numbers for poly(C)$_{20}$ and poly(G)$_{20}$ were ~450. Moreover, the interaction energies between different ssDNA and MoS_2 surfaces were computed in Fig. 3(d). Poly(A)$_{20}$ showed the strongest interaction with the MoS_2 surface, with the interaction energy reaching –1900 kJ·mol^{-1}, while poly (C)$_{20}$ showed the weakest interaction energy of approximately –1300 kJ·mol^{-1}. By calculating the interaction energy versus the number of adsorbed residues, we could conclude that the binding strength of single base to MoS_2 was in the order of G > A > C > T, which was in agreement with previous computation results [32,41].

3.3 ssDNA passes through the Mo only MoS_2 nanopore

Figure 4 aims to investigate how the transmembrane bias affects ssDNA translocation. It clearly shows the translocation traces of four ssDNAs through the Mo only nanopore under the driving voltage of 0.5, 0.8 and 1.2 V, which was defined as the number of bases passing through the middle plane of the MoS_2 membrane over time. All ssDNAs translocated through the Mo only nanopore in a stepwise manner, as reported in previous studies on peptide or DNA passing through various nanopores [30,59,61,62]. The ssDNA translocations contained long stationary pauses dotted with short, quick steps. Furthermore, the time taken by the ssDNA to completely translocate through

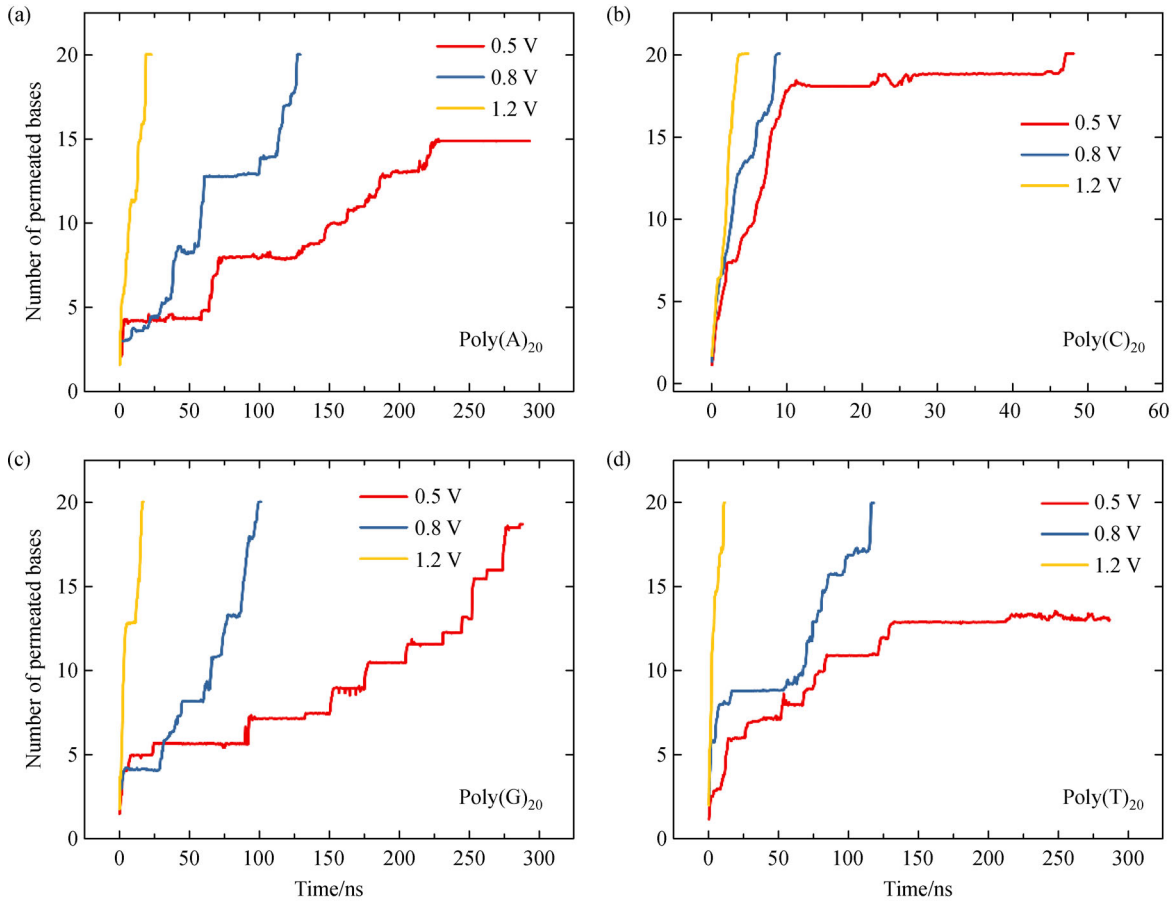

Fig. 4 The translocation traces of ssDNA driven through Mo only nanopore by different voltages of 0.5 V, 0.8 V and 1.2 V: (a) poly $(A)_{20}$, (b) poly$(C)_{20}$, (c) poly$(G)_{20}$ and (d) poly$(T)_{20}$.

the nanopore decreased dramatically with increasing voltage. At low voltage, the time span between two translocation events, as indicated by a sudden change in translocation number, was quite large, and thus the residence time of ssDNA bases in the nanopores was quite long. At high voltage, the translocation process showed a fast translocation step and short residence time and still had a stepwise fashion. Under the voltage of 0.5 V, poly$(A)_{20}$, poly$(T)_{20}$ and poly$(G)_{20}$ did not completely pass through the Mo only nanopore within 300 ns, while poly$(C)_{20}$ completely penetrated through the nanopore within 50 ns. This finding agrees with the weakest adsorption of poly$(C)_{20}$ on MoS_2 (Fig. 3(d)). When the voltage increased to 0.8 V, the translocation time was shortened by more than one half. When the voltage reached 1.2 V, all four ssDNA species completed the translocation process within 25 ns.

Furthermore, each of the above simulations (see Fig. 4) was repeated three times, and the average translocation speed of ssDNA at different voltages is shown in Fig. 5. It was found that at the same voltage, the order of translocation speed for the four ssDNAs was poly$(A)_{20}$ < poly$(T)_{20}$ < poly$(G)_{20}$ < poly$(C)_{20}$; this order

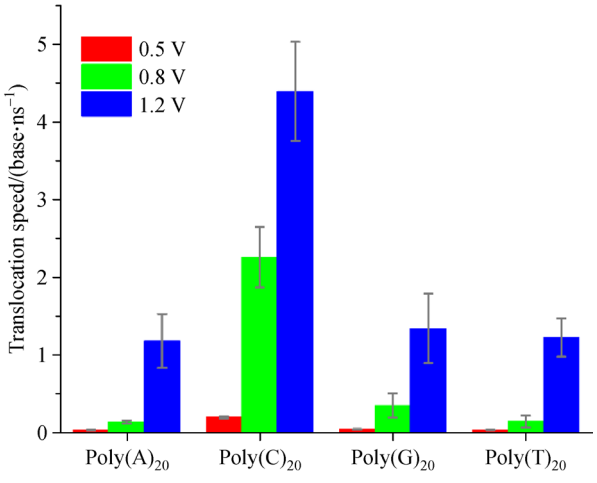

Fig. 5 The translocation speeds of ssDNA (poly$(A)_{20}$, poly$(C)_{20}$, poly$(G)_{20}$ and poly$(T)_{20}$) driven through Mo only nanopore by different voltages.

is opposite to the order of interaction strength between the ssDNA and MoS_2 surface. The transmembrane voltage affected the translocation speed of poly$(C)_{20}$ even more

significantly.

The ionic current during the ssDNA translocation process was calculated. Figure 6 illustrates the ionic current of four ssDNAs passing through the Mo only nanopore versus the simulation time at a biased voltage of 0.8 V. After ssDNA completely passed through the pore, the ion current restored to the opening current. The insets in Fig. 6 show different snapshots of ssDNA in the Mo only nanopore, and the arrow refers to the corresponding instantaneous ionic current. When there was only one base in the nanopore, the blocking degree of ionic current was relatively small, but blocking degree was different for various bases. For instance, the blocking amplitude of ionic current for poly(A)$_{20}$ and poly(G)$_{20}$ at 3 ns was 26% and 37%, respectively. When the number of bases in the nanopore reached 2 or 3, the ionic current was significantly blocked, almost approaching 0 nA, e.g., the ionic current values of poly(C)$_{20}$, poly(A)$_{20}$, poly(G)$_{20}$ and poly(T)$_{20}$ at 4.5, 38, 50 and 73 ns, respectively. Interestingly, when the midpart of two bases occupied the nanopore, the ionic current was blocked less, such as poly(A)$_{20}$ and poly(T)$_{20}$ at 77 and 26 ns, respectively. By identifying the translocated base and ion current changes over time, each penetration pause yielded quite a stable ionic current. The blocked ionic current and the stepwise movement of ssDNA indicated promising application potential for DNA-sequencing. Well-defined signals could be produced from the long pauses in the translocation process to read the base content in the nanopore. Although Fig. 4 shows a pause time at tens of nanoseconds, it could be prolonged to microseconds by further lowering the transmembrane bias.

3.4 ssDNA passes through the S only MoS_2 nanopore

As shown in Fig. 7, ssDNAs were driven through the S only nanopore by biased voltage. Figure 7 shows the time series of the translocation number of four ssDNAs through the S only MoS_2 nanopore under a driving voltage of 0.8, 1.2 and 2.4 V. It was observed that only 4–6 bases could pass through the S only nanopore at 0.8 V even after a long simulation time of 400 ns. When the voltage increased to 1.2 V, the translocation number of poly(A)$_{20}$ and poly(G)$_{20}$ increased slightly to ~7, while those of poly(C)$_{20}$ and poly(T)$_{20}$ rose to above 12. Under 2.4 V, the four ssDNAs fully permeated within 70 ns. Comparing with Mo only nanopore, ssDNA passed through S only nanopore very slowly. The time span of two translocation events at low voltage (0.5 or 0.8 V) for S only nanopore was very long,

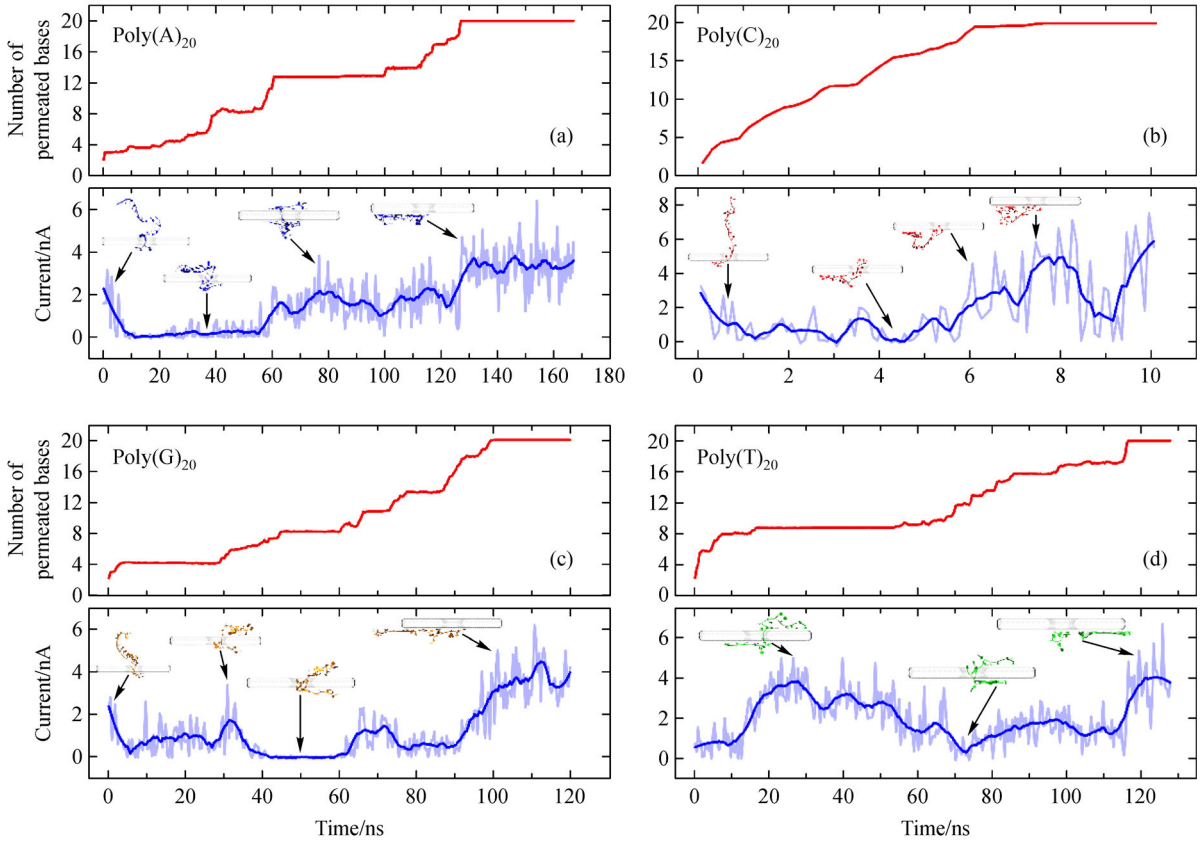

Fig. 6 The changes in translocation base number and ionic current of ssDNA over time driven through Mo only nanopore at a 0.8 V bias: (a) poly(A)$_{20}$, (b) poly(C)$_{20}$, (c) poly(G)$_{20}$ and (d) poly(T)$_{20}$. The insets show the instantaneous conformation corresponding to the ionic current values.

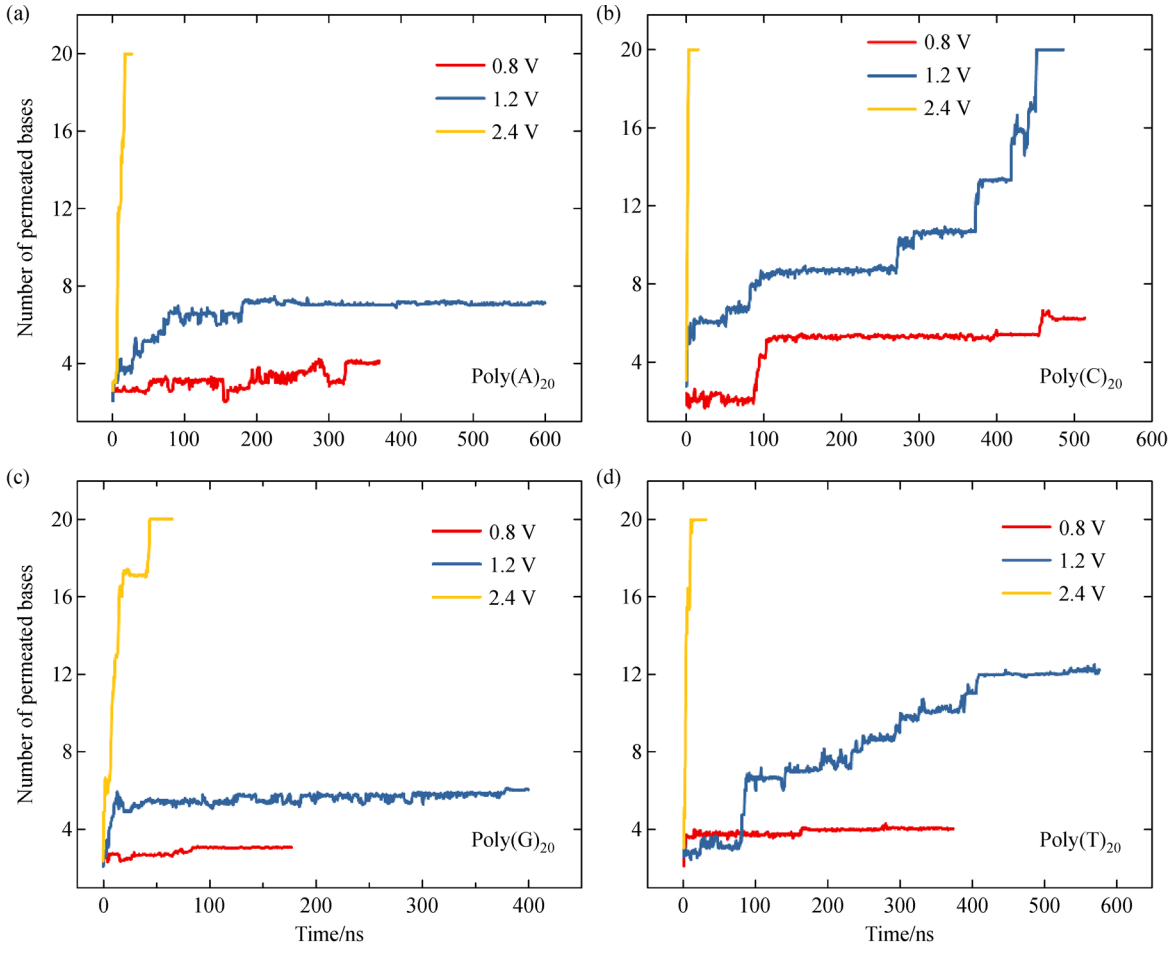

Fig. 7 The translocation traces of ssDNA driven through S only nanopore by different voltages: (a) poly(A)$_{20}$, (b) poly(C)$_{20}$, (c) poly(G)$_{20}$ and (d) poly(T)$_{20}$.

though it was significantly reduced at voltages above 1.2 V. Such low translocation speeds could be attributed to the negatively charged S atom repelling the negatively charged base from translocating, resulting in a high energy barrier for the translocation of ssDNA [26,63]. In contrast, because Mo atoms were positively charged, the translocation energy barrier of ssDNA through Mo nanopore was lower [20].

In Fig. 7, the influence of increasing voltage on the perforation time of the four ssDNAs followed this order: poly(C)$_{20}$ > poly(T)$_{20}$ > poly(A)$_{20}$ > poly(G)$_{20}$. Meanwhile, the averaged translocation speed of ssDNA at different voltages for three repeated simulations was presented in Fig. 8, showing an order of poly(C)$_{20}$ > poly(T)$_{20}$ > poly(A)$_{20}$ > poly(G)$_{20}$.

Figure 9 recorded the ionic current trajectory when ssDNA passed through the S only nanopore at 2.4 V. From Fig. 9, poly(A)$_{20}$ and poly(T)$_{20}$ showed the strongest blocking effect on the ionic current. After the ssDNA was completely penetrated, the ionic current increased to the level of an open nanopore. The insets in Fig. 9 represent

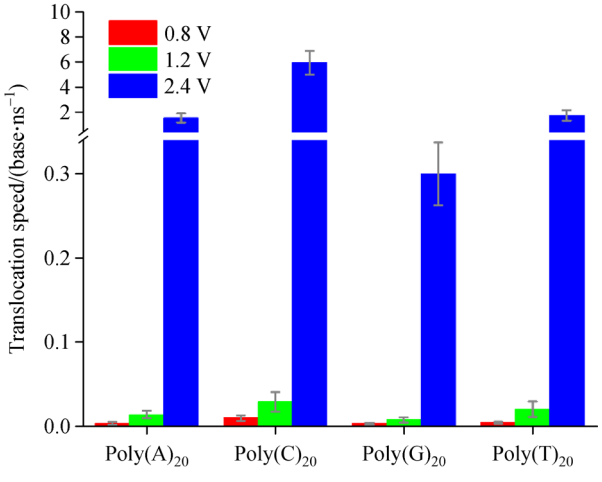

Fig. 8 The translocation speeds of ssDNA driven through S only nanopore by different voltages: poly(A)$_{20}$, poly(C)$_{20}$, poly(G)$_{20}$ and poly(T)$_{20}$.

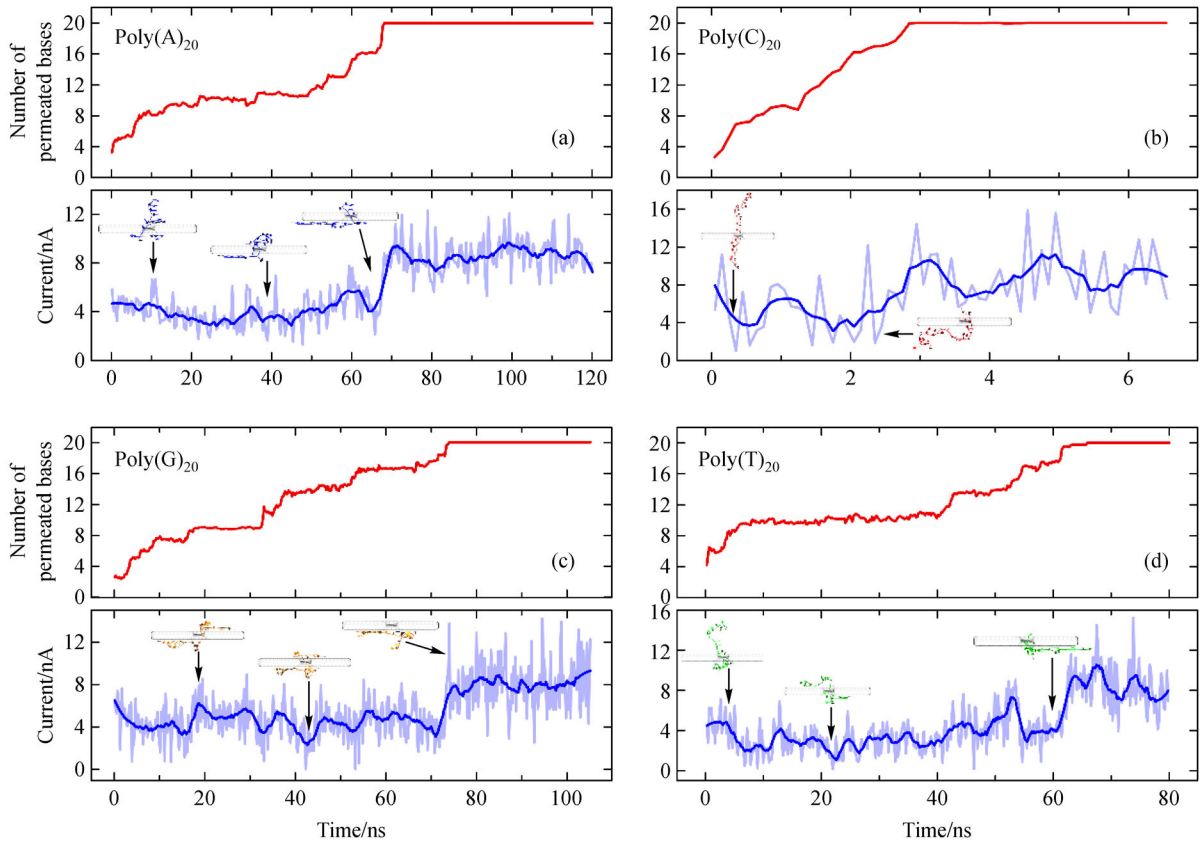

Fig. 9 The translocation traces and ionic current blockages of ssDNA driven through S only nanopore at a 2.4 V bias: (a) poly(A)$_{20}$, (b) poly(C)$_{20}$, (c) poly(G)$_{20}$ and (d) poly(T)$_{20}$.

the instantaneous conformations of ssDNA at different simulation times, and the arrow refers to the corresponding ionic current. For example, the blocking ranges were less than 20% for poly(A)$_{20}$ and poly(G)$_{20}$, as illustrated in the first inset of ionic current trajectory. When the center of the nanopore was blocked by bases, the degree of ionic current blocking increased. When the number of bases in the nanopore reached 2–3, the obstruction degree of ionic current was more evident, which almost reduced to 0 nA, as shown in the second inset of poly(A)$_{20}$, poly(G)$_{20}$ and poly(T)$_{20}$.

3.5 ssDNA passes through the Mixed MoS_2 nanopore

Figure 10 shows the four ssDNAs translocating through the Mixed MoS_2 nanopore at different voltages. At a voltage of 0.8 V, only 4–6 bases of poly(A)$_{20}$, poly(G)$_{20}$ and poly(T)$_{20}$ could permeate through the nanopore during a long simulation time of 400 ns, while poly(C)$_{20}$ completely translocated through the nanopore within 100 ns. When the voltage increased to 1.2 V, poly(A)$_{20}$ and poly(T)$_{20}$ completely passed through the nanopore within 400 ns; poly(C)$_{20}$ translocated completely within 50 ns (~1/2 of the time at 0.8 V), while the translocation number of poly(G)$_{20}$ did not change much. For the voltage rising to 2.4 V, all four ssDNAs entirely permeated within 40 ns. The translocation process of ssDNA became much faster at high voltages but retained the stepwise character. The ssDNA passed through the Mixed nanopore faster than that in the S only nanopore, but slower than that in the Mo only nanopore. This finding may be attributed to the positively charged Mo atoms weakening the energy barrier through the Mixed nanopore.

Moreover, as shown in Fig. 10, it was found that the influence of increasing voltage on the translocation time of the four ssDNAs was poly(C)$_{20}$ > poly(T)$_{20}$ > poly(A)$_{20}$ > poly(G)$_{20}$. The averaged translocation speed of ssDNA at different voltages is also displayed in Fig. 11. At the same voltage, the permeation speed of ssDNA followed the order of poly(C)$_{20}$ > poly(T)$_{20}$ > poly(A)$_{20}$ > poly(G)$_{20}$. Figure 12 shows the translocation trajectories and ionic currents of four ssDNAs translocating through the Mixed MoS_2 nanopore (the driving bias was 2.4 V for poly(G)$_{20}$ whose translocation speed was extremely slow, but 1.2 V for other ssDNAs). The poly(A)$_{20}$ and poly(G)$_{20}$ exhibited the maximum ionic blockages. These simulation results revealed that well-defined ionic current blockages could be produced from the stepwise translocation of

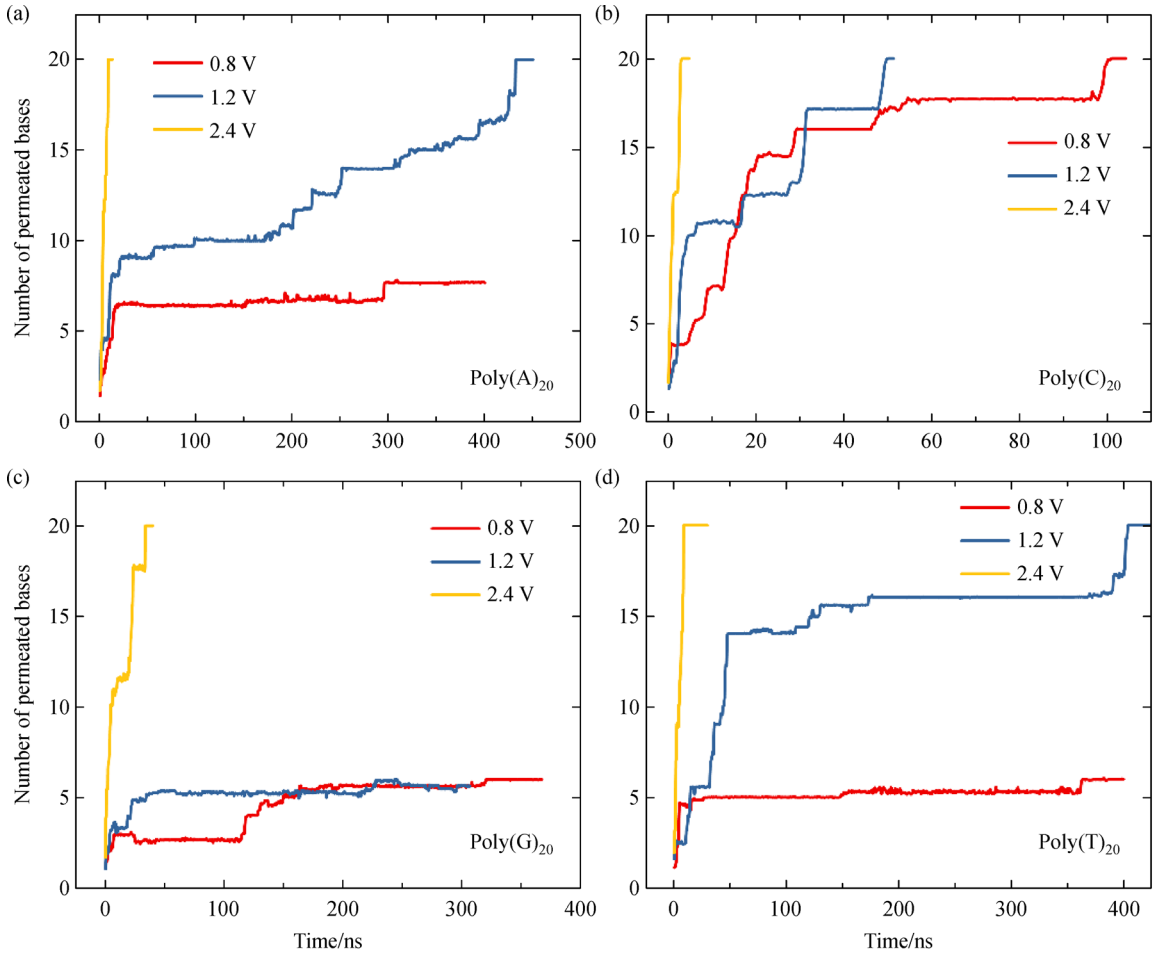

Fig. 10 The translocation traces of ssDNA driven through Mixed nanopore by different voltages: (a) poly(A)$_{20}$, (b) poly(C)$_{20}$, (c) poly(G)$_{20}$ and (d) poly(T)$_{20}$.

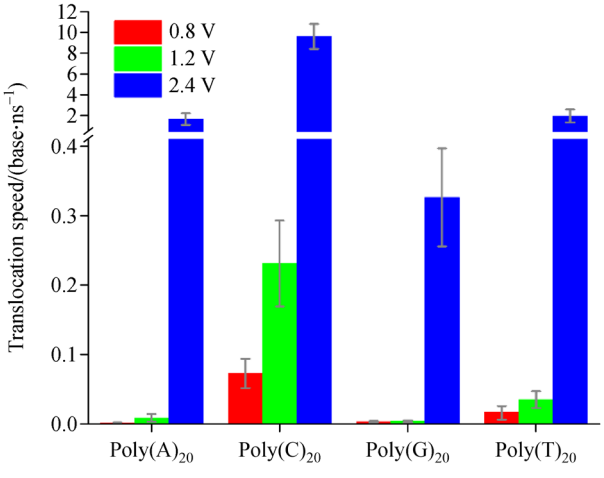

Fig. 11 The translocation speeds of ssDNA driven through the Mixed nanopore by different voltages: poly(A)$_{20}$, poly(C)$_{20}$, poly(G)$_{20}$ and poly(T)$_{20}$.

ssDNA through a MoS_2 nanopore, which can be employed to identify the DNA sequence. The ionic current in the experiments may be even better defined because 1) the applied bias could be lowered to prolong the measuring time to the order of microseconds (which is unfeasible for current MD simulations) and 2) the experimental system could be much larger to reduce the random noise in the signal.

4 Conclusions

In this work, extensive MD simulations were performed to study the ssDNA translocation through different MoS_2 nanopores, with implications for nanopore based DNA sequencing. All of the studied ssDNAs adsorbed to the MoS_2 surface and passed through the MoS_2 nanopores in a stepwise manner as driven by an external transmembrane bias. Such stepwise translocation led to well-defined ionic currents relevant to the content of the ssDNA fragment in

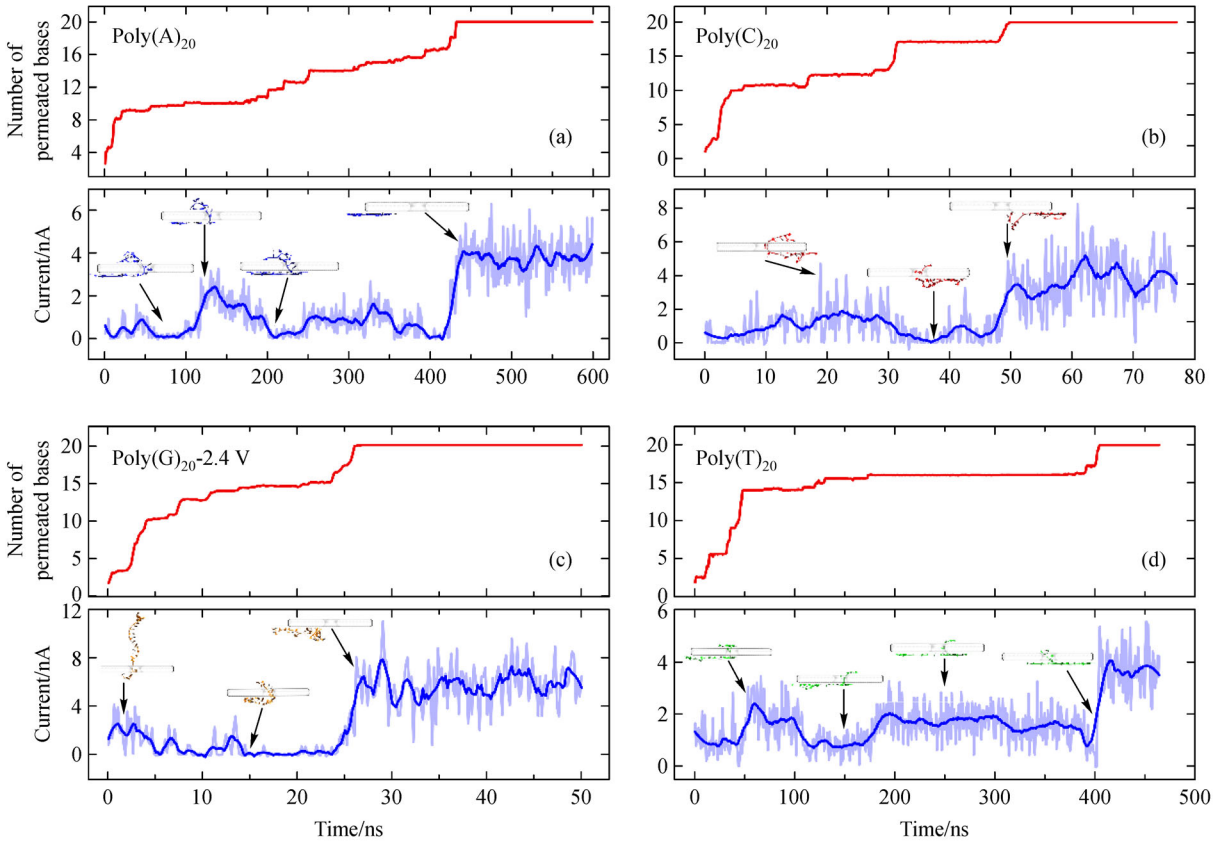

Fig. 12 The translocation traces and ionic current blockages of ssDNA driven through a Mixed nanopore at a 1.2 V bias: (a) poly(A)$_{20}$, (b) poly(C)$_{20}$, (c) poly(G)$_{20}$ (2.4 V) and (d) poly(T)$_{20}$.

the nanopore and thus could be employed to read ssDNA sequences. The ionic current signal in the experiments could be further improved by employing much longer measuring times and larger measuring systems, which may diminish the noise. Compared with other DNA sequencing methods [64,65], this MoS_2 nanopore-based DNA sequencing method is simple and quick and does not require any other chemical reagent in principle. The translocation speed of ssDNAs could be regulated by the bias and its interaction with MoS_2, e.g., high voltage or the weak binding affinity of C base (e.g., the C base of DNA) with MoS_2 surface would lead to fast translocation. Furthermore, the structure of MoS_2 nanopores regulated the translocation process and the ionic current considerably, e.g., the S only nanopore produced the largest open-pore ionic current, while the positively charged Mo only nanopore yielded the highest translocation speed of ssDNA. This work provided not only a proof of concept design for DNA sequencing with a MoS_2 nanopore but also valuable considerations when implementing such design with experiments, e.g., fine tuning the DNA sequencing performance, such as the translocation speed and the ionic current, by engineering the nanopore structure.

Acknowledgements The financial support from the Science and Technology Key Project of Guangdong Province (No. 2020B010188002), Guangdong Natural Science Foundation (No. 2019A1515011121), Guangzhou Technology Project (No. 201804010219), the National Natural Science Foundation of China (Grant Nos. 21908046 and 22078104), Hubei Natural Science Foundation (No. 2019CFB293), Guangdong Basic and Applied Basic Research Foundation (No. 2019A1515110706), State Key Laboratory of Pulp and Paper Engineering (No. SCUT201828) and the Fundamental Research Funds for the Central Universities were gratefully acknowledged.

References

1. Ying Y L, Long Y T. Nanopore-based single-biomolecule interfaces: from information to knowledge. Journal of the American Chemical Society, 2019, 141(40): 15720–15729
2. Ameur A, Kloosterman W P, Hestand M S. Single-molecule sequencing: towards clinical applications. Trends in Biotechnology, 2019, 37(1): 72–85
3. Varongchayakul N, Song J, Meller A, Grinstaff M W. Single-molecule protein sensing in a nanopore: a tutorial. Chemical Society Reviews, 2018, 47(23): 8512–8524
4. Keyser U F. Enhancing nanopore sensing with DNA nanotechnology. Nature Nanotechnology, 2016, 11(2): 106–108
5. Shi W, Friedman A K, Baker L A. Nanopore sensing. Analytical

Chemistry, 2017, 89(1): 157–188
6. Ying Y, Gao R, Hu Y, Long Y. Electrochemical confinement effects for innovating new nanopore sensing mechanisms. Small Methods, 2018, 2(6): 1700390
7. Cao C, Ying Y L, Hu Z L, Liao D F, Tian H, Long Y T. Discrimination of oligonucleotides of different lengths with a wild-type aerolysin nanopore. Nature Nanotechnology, 2016, 11(8): 713–718
8. Cao C, Liao D F, Yu J, Tian H, Long Y T. Construction of an aerolysin nanopore in a lipid bilayer for single-oligonucleotide analysis. Nature Protocols, 2017, 12(9): 1901–1911
9. Soni G V, Dekker C. Detection of nucleosomal substructures using solid-state nanopores. Nano Letters, 2012, 12(6): 3180–3186
10. Li J, Tang Z P, Hu R, Fu Q, Yan E F, Wang S Y, Guo P X, Zhao Q, Yu D P. Probing surface hydrophobicity of individual protein at single-molecule resolution using solid-state nanopores. Science China Materials, 2015, 58(6): 455–466
11. Lee K, Park K B, Kim H J, Yu J S, Chae H, Kim H M, Kim K B. Recent progress in solid-state nanopores. Advanced Materials, 2018, 30(42): e1704680
12. Hu R, Zhu H. Graphene-based membranes for organic solvent nanofiltration. Science China Materials, 2018, 61(3): 429–431
13. Siwy Z S, Davenport M. Graphene opens up to DNA. Nature Nanotechnology, 2010, 5(10): 697–698
14. Branton D, Deamer D W, Marziali A, Bayley H, Benner S A, Butler T, Di Ventra M, Garaj S, Hibbs A, Huang X, et al. The potential and challenges of nanopore sequencing. Nature Biotechnology, 2008, 26 (10): 1146–1153
15. Schneider G F, Kowalczyk S W, Calado V E, Pandraud G, Zandbergen H W, Vandersypen L M, Dekker C. DNA translocation through graphene nanopores. Nano Letters, 2010, 10(8): 3163–3167
16. Wilson J, Sloman L, He Z, Aksimentiev A. Graphene nanopores for protein sequencing. Advanced Functional Materials, 2016, 26(27): 4830–4838
17. Heerema S J, Dekker C. Graphene nanodevices for DNA sequencing. Nature Nanotechnology, 2016, 11(2): 127–136
18. Traversi F, Raillon C, Benameur S M, Liu K, Khlybov S, Tosun M, Krasnozhon D, Kis A, Radenovic A. Detecting the translocation of DNA through a nanopore using graphene nanoribbons. Nature Nanotechnology, 2013, 8(12): 939–945
19. Liu K, Feng J, Kis A, Radenovic A. Atomically thin molybdenum disulfide nanopores with high sensitivity for DNA translocation. ACS Nano, 2014, 8(3): 2504–2511
20. Farimani A B, Min K, Aluru N R. DNA base detection using a single-layer MoS_2. ACS Nano, 2014, 8(8): 7914–7922
21. Feng J, Liu K, Bulushev R D, Khlybov S, Dumcenco D, Kis A, Radenovic A. Identification of single nucleotides in MoS_2 nanopores. Nature Nanotechnology, 2015, 10(12): 1070–1076
22. Arjmandi-Tash H, Belyaeva L A, Schneider G F. Single molecule detection with graphene and other two-dimensional materials: nanopores and beyond. Chemical Society Reviews, 2016, 45(3): 476–493
23. Husale B S, Sahoo S, Radenovic A, Traversi F, Annibale P, Kis A. ssDNA binding reveals the atomic structure of graphene. Langmuir, 2010, 26(23): 18078–18082
24. Radisavljevic B, Radenovic A, Brivio J, Giacometti V, Kis A. Single-layer MoS_2 transistors. Nature Nanotechnology, 2011, 6(3): 147–150
25. Feng J, Liu K, Graf M, Lihter M, Bulushev R D, Dumcenco D, Alexander D T, Krasnozhon D, Vuletic T, Kis A, Radenovic A. Electrochemical reaction in single layer MoS_2: nanopores opened atom by atom. Nano Letters, 2015, 15(5): 3431–3438
26. Heiranian M, Farimani A B, Aluru N R. Water desalination with a single-layer MoS_2 nanopore. Nature Communications, 2015, 6(1): 8616
27. Heckl W M, Smith D P, Binnig G, Klagges H, Hänsch T W, Maddocks J. Two-dimensional ordering of the DNA base guanine observed by scanning tunneling microscopy. Proceedings of the National Academy of Sciences of the United States of America, 1991, 88(18): 8003–8005
28. Liang L, Shen J W, Zhang Z, Wang Q. DNA sequencing by two-dimensional materials: as theoretical modeling meets experiments. Biosensors & Bioelectronics, 2017, 89(Pt 1): 280–292
29. Sathe C, Zou X Q, Leburton J P, Schulten K. Computational investigation of DNA detection using graphene nanopores. ACS Nano, 2011, 5(11): 8842–8851
30. Chen H, Li L, Zhang T, Qiao Z W, Tang J, Zhou J. Protein translocation through a MoS_2 nanopore: a molecular dynamics study. Journal of Physical Chemistry C, 2018, 122(4): 2070–2080
31. Xu Z, Zhang S, Weber J K, Luan B, Zhou R, Li J. Sequential protein unfolding through a carbon nanotube pore. Nanoscale, 2016, 8(24): 12143–12151
32. Luan B, Zhou R. Spontaneous transport of single-stranded DNA through graphene-MoS_2 heterostructure nanopores. ACS Nano, 2018, 12(4): 3886–3891
33. Heerema S J, Schneider G F, Rozemuller M, Vicarelli L, Zandbergen H W, Dekker C. 1/f noise in graphene nanopores. Nanotechnology, 2015, 26(7): 074001
34. Zhou W Q, Qiu H, Guo Y F, Guo W L. Molecular insights into distinct detection properties of α-hemolysin, MspA, CsgG, and aerolysin nanopore sensors. Journal of Physical Chemistry B, 2020, 124(9): 1611–1618
35. Lin Z, Chen H, Dong J, Zhao D, Li L. Nanopore-based biomolecular detection. Progress in Chemistry, 2020, 32(5): 562–580 (in Chinese)
36. Deng S, Hu H, Zhuang G, Zhong X, Wang J. A strain-controlled C_2N monolayer membrane for gas separation in PEMFC application. Applied Surface Science, 2018, 441: 408–414
37. Cao L, Ren H, Miao J, Guo W, Li Y, Li G. Validation of polarizable force field parameters for nucleic acids by inter-molecular interactions. Frontiers of Chemical Science and Engineering, 2016, 10(2): 203–212
38. Yuan L, Wu H, Zhao Y, Qin X, Li Y. Molecular simulation of the interaction mechanism between CodY protein and DNA in *Lactococcus lactis*. Frontiers of Chemical Science and Engineering, 2019, 13(1): 133–139
39. Liang L J, Cui P, Wang Q, Wu T, Agren H, Tu Y Q. Theoretical study on key factors in DNA sequencing with graphene nanopores. RSC Advances, 2013, 3(7): 2445–2453
40. Hanwell M D, Curtis D E, Lonie D C, Vandermeersch T, Zurek E, Hutchison G R. Avogadro: an advanced semantic chemical editor, visualization, and analysis platform. Journal of Cheminformatics, 2012, 4(1): 17

41. Liang L, Hu W, Xue Z, Shen J. Theoretical study on the interaction of nucleotides on two-dimensional atomically thin graphene and molybdenum disulfide. FlatChem, 2017, 2: 8–14
42. Jorgensen W L, Chandrasekhar J, Madura J D, Impey R W, Klein M L. Comparison of simple potential functions for simulating liquid water. Journal of Chemical Physics, 1983, 79(2): 926–935
43. Hess B, Kutzner C, Van Der Spoel D, Lindahl E. Gromacs 4: algorithms for highly efficient, load-balanced, and scalable molecular simulation. Journal of Chemical Theory and Computation, 2008, 4(3): 435–447
44. MacKerell A D Jr, Bashford D, Bellott M, Dunbrack R L Jr, Evanseck J D, Field M J, Fischer S, Gao J, Guo H, Ha S, et al. All-atom empirical potential for molecular modeling and dynamics studies of proteins. Journal of Physical Chemistry B, 1998, 102(18): 3586–3616
45. Humphrey W, Dalke A, Schulten K. VMD: visual molecular dynamics. Journal of Molecular Graphics & Modelling, 1996, 14(1): 33–38
46. Feng J, Graf M, Liu K, Ovchinnikov D, Dumcenco D, Heiranian M, Nandigana V, Aluru N R, Kis A, Radenovic A. Single-layer MoS_2 nanopores as nanopower generators. Nature, 2016, 536(7615): 197–200
47. Hess B, Bekker H, Berendsen H J, Fraaije J G. LINCS: a linear constraint solver for molecular simulations. Journal of Computational Chemistry, 1997, 18(12): 1463–1472
48. Miyamoto S, Kollman P A. Settle: an analytical version of the SHAKE and RATTLE algorithm for rigid water models. Journal of Computational Chemistry, 1992, 13(8): 952–962
49. Qiu H, Sarathy A, Schulten K, Leburton J P. Detection and mapping of DNA methylation with 2D material nanopores. npj 2D Materials and Applications, 2017, 1(3): 1–8
50. Allen M P, Tildesley D J. Computer Simulation of Liquids. 1st ed. Oxford, UK: Clarendon Press, 1987, 385–386
51. Darden T, York D, Pedersen L. Particle mesh Ewald: an $N\cdot\log(N)$ method for Ewald sums in large systems. Journal of Chemical Physics, 1993, 98(12): 10089–10092
52. Bussi G, Donadio D, Parrinello M. Canonical sampling through velocity rescaling. Journal of Chemical Physics, 2007, 126(1): 014101
53. Berendsen H J C, Postma J P M, Van Gunsteren W F, DiNola A, Haak J R. Molecular dynamics with coupling to an external bath. Journal of Chemical Physics, 1984, 81(8): 3684–3690
54. Cheng A, Merz K M. Application of the NoséHoover chain algorithm to the study of protein dynamics. Journal of Physical Chemistry, 1996, 100(5): 1927–1937
55. Li L B, Duan Y F, Liao S W, Ke Q, Qiao Z W, Wei Y Y. Adsorption and separation of propane/propylene on various ZIF-8 polymorphs: insights from GCMC simulations and the ideal adsorbed solution theory (IAST). Chemical Engineering Journal, 2020, 386: 123945
56. Li L, Vorobyov I, Allen T W. Potential of mean force and pKa profile calculation for a lipid membrane-exposed arginine side chain. Journal of Physical Chemistry B, 2008, 112(32): 9574–9587
57. Li L B, Zhang T, Duan Y F, Wei Y Y, Dong C J, Ding L, Qiao Z W, Wang H H. Selective gas diffusion in two-dimensional MXene lamellar membranes: insights from molecular dynamics simulations. Journal of Materials Chemistry. A, Materials for Energy and Sustainability, 2018, 6(25): 11734–11742
58. Zhao D, Li L, He D, Zhou J. Molecular dynamics simulations of conformation changes of HIV-1 regulatory protein on graphene. Applied Surface Science, 2016, 377: 324–334
59. Barati Farimani A, Dibaeinia P, Aluru N R. DNA origami-graphene hybrid nanopore for DNA detection. ACS Applied Materials & Interfaces, 2017, 9(1): 92–100
60. Balasubramanian R, Pal S, Joshi H, Rao A, Naik A, Varma M, Chakraborty B, Maiti P K. DNA translocation through hybrid bilayer nanopores. Journal of Physical Chemistry C, 2019, 123(18): 11908–11916
61. Qiu H, Sarathy A, Leburton J P, Schulten K. Intrinsic stepwise translocation of stretched ssDNA in graphene nanopores. Nano Letters, 2015, 15(12): 8322–8330
62. Chu J, Gonzalez Lopez M, Cockroft S L, Amorin M, Ghadiri M R. Real-time monitoring of DNA polymerase function and stepwise single-nucleotide DNA strand translocation through a protein nanopore. Angewandte Chemie International Edition, 2010, 49 (52): 10106–10109
63. Ling Y, Gu Z, Kang S, Luo J, Zhou R. Structural damage of a β-sheet protein upon adsorption onto molybdenum disulfide nanotubes. Journal of Physical Chemistry C, 2016, 120(12): 6796–6803
64. Zhang J, Wu S, Ma L, Wu P, Liu J. Graphene oxide as a photocatalytic nuclease mimicking nanozyme for DNA cleavage. Nano Research, 2020, 13(2): 455–460
65. Xu Y, Wang H, Chen B, Liu H, Zhao Y. Emerging barcode particles for multiplex bioassays. Science China Materials, 2019, 62(3): 289–324